electronics

MDPI

Article

An Adaptive Backstepping Sliding Mode Cascade-Control Method for a DC Microgrid Based on Nonlinear Virtual Inertia

Jingfeng Mao, Xiaotong Zhang, Tengfei Dai, Aihua Wu * and Chunyun Yin

School of Electrical Engineering, Nantong University, Nantong 226019, China; mao.jf@ntu.edu.cn (J.M.); 2011310005@stmail.ntu.edu.cn (X.Z.); 1912310010@stmail.ntu.edu.cn (T.D.); 2011310020@stmail.ntu.edu.cn (C.Y.)
* Correspondence: wu.ah@ntu.edu.cn

Abstract: In order to improve the bus voltage robustness of distributed multi-source DC microgrid, a new cascade control method based on nonlinear virtual inertia and adaptive backstepping sliding mode is proposed. Firstly, the mathematical model of distributed multi-source DC microgrid with a buck–boost interface converter is analyzed and established. A nonlinear virtual inertia control method based on a variable droop coefficient is given by introducing the converter output voltage variation rate feedback term and a saturation function equation. Secondly, the voltage and current double closed-loop cascade controller is designed by using backstepping sliding mode control and adaptive algorithms. Finally, the system and cascade control models are built in MATLAB/Simulink for multi-case simulation. The feasibility and effectiveness of the proposed method is verified by comparing the results with traditional control methods.

Keywords: DC microgrid; virtual inertia; droop control; backstepping sliding mode control; adaptive control

Citation: Mao, J.; Zhang, X.; Dai, T.; Wu, A.; Yin, C. An Adaptive Backstepping Sliding Mode Cascade-Control Method for a DC Microgrid Based on Nonlinear Virtual Inertia. *Electronics* **2021**, *10*, 3100. https://doi.org/10.3390/electronics10243100

Academic Editor: Ali Mehrizi-Sani

Received: 5 November 2021
Accepted: 10 December 2021
Published: 13 December 2021

1. Introduction

When distributed generation is connected to the grid, the DC microgrid can provide a flexible and efficient basic distribution layer. The DC microgrid has received more and more attention for avoiding the conversion of multi-stage power electronic converters such as AC/DC and DC/AC, as well as the complex frequency and reactive power regulation problems [1–3].

The main control goal of the DC microgrid is the stability of the DC bus voltage. Compared to master-slave control, which relies on high-speed communication technology, droop control does not require communication [4]. DC microgrid systems with droop control have higher reliability and can easily realize power distribution and voltage regulation among multiple sources [5,6]. However, the DC microgrid is composed of a large number of power electronic converters, and its inertia is insufficient. When it is disturbed, it is easy to cause large dynamic voltage fluctuations [7,8]. Therefore, it is not only necessary to consider improving the transient control performance of the voltage closed-loop but also to analyze and solve the problem of insufficient system inertia when designing a DC microgrid bus voltage controller. Although increasing the DC bus capacity can increase the inertia of the DC microgrid and reduce the voltage transient caused by the sudden change of source load power, and it is beneficial to the system's stable operation effect. However, considering the high cost and large volume of power capacitors, the concept of virtual inertia is a major alternative [9,10].

The concept of virtual inertia comes from the AC microgrid, which is based on the virtual inertia compensation of virtual synchronous generators. The DC microgrid learns from it and uses the equivalent concept to improve inertia. In the AC microgrid, the realization of virtual inertia utilizes the change of the frequency, while in the DC microgrid, it is realized by the change of the DC voltage. To reasonably use the degree of voltage change and compensate the system with appropriate virtual inertia, this paper proposes a

variable droop coefficient nonlinear virtual inertia control method considering the voltage change rate. The droop control method used by the converter is equivalent to the series virtual impedance [11]. It uses load fluctuation feedback to affect the nonlinear change of the droop coefficient, and the bus makes nonlinear adjustments regarding the output voltage. As a result, the voltage stabilization inertia of the distributed power supply with the buck–boost converter interface is improved.

In addition, the DC/DC converter is a key executive component in the DC microgrid, and it is used for the output power control and the voltage regulation of distributed generation. There are many types of DC/DC converters. Among them, the traditional buck–boost converter has both a buck–boost function, and it has the advantages of a small number of components and low cost. The buck–boost converter has been widely used in various fields of research, such as energy storage systems, electric vehicle drives systems, photovoltaic power generation systems, etc. However, the buck–boost converter is a highly nonlinear system; there is a right half-plane zero in the classic control theory. Therefore, we need to explore the nonlinear control method of the converter more deeply to improve the outstanding high-frequency dynamic output characteristics of the converter. This is not only an important issue that needs to be further resolved but also a key technology for stabilizing the DC bus voltage [12–17].

To solve the problem that negative incremental impedance of a constant power load can lead to system instability, a higher-order sliding mode control method based on a super-torque algorithm was proposed in the reference [18]. In a medium-voltage DC integrated power system, it is experimentally demonstrated that the converter has strong robustness and reduced chattering in the system under the disturbances of sudden load changes, but the controller only involves single closed-loop voltage control and lacks regulation of the inductor current, which may cause current spikes during operating mode transitions. Reference [19] studied the dynamic control characteristics of buck–boost converter based on hysteresis current. This reference uses a single closed-loop current-based method for power control. The characteristic of this controller is that the structure is simple and easy to realize.

However, there are usually two types of converter output voltage regulation control strategies, which are divided into single closed-loop and multi-closed-loop cascades. The cascade control method introduces internal current feedback to improve response speed and limit overcurrent [20]. Because the multi-closed-loop cascade control method can integrate the advantages of multiple types of control strategies, it is more reliable and efficient. Reference [21] proposed a multi-PI loop cascade control method for buck–boost converter. However, conventional PI control has some shortcomings: poor robustness, easy oscillation and saturation of the control volume. The external voltage loop and internal current loop in reference [22] both adopt non-singular terminal sliding mode control. This control method is easy to meet the fixed switching frequency requirements and demonstrates the strong robustness of sliding mode control. The reference [23] proposes a cascade control scheme with a conventional droop control method for the outermost control and an internal cascade control scheme consisting of a voltage derivative control inner loop and a voltage control outer loop. The control method achieves accurate power-sharing and proper voltage regulation of the DC microgrid in islanded operation mode. However, due to the presence of cable impedance, the traditional droop control suffers from a contradiction between voltage deviation and current distribution accuracy. In order to improve the limitations of conventional droop control, secondary control is proposed in the form of compensation to readjust the initial droop profile. A cascade control scheme consisting of virtual inertia control, recovery control and coordinated current sharing control is proposed in the reference [24]. During grid-connected and off-grid operation of the DC microgrid, both transient and steady-state voltage conditions at the DC bus are significantly improved when there are abrupt changes at the supply and load sides. However, the control method does not take into account the nonlinear effects of virtual inertia control during mode switching. For multiple parallel buck–boost converters with parallel power supplies, the

reference [25] proposes a DC microgrid cascade control scheme with good scalability and robustness, which consists of a droop controller and an auxiliary controller, not only for current sharing between parallel power supplies, but also for compensating the voltage deviation caused by the main controller. However, the cascade control only involves the compensation control of voltage deviation, but not the regulation of inductor current, which cannot avoid the influence of inductor spike current to the system.

In recent years, control strategies based on sliding mode and backstepping have been widely used in various types of control systems due to their excellent adaptability and strong robustness. For nonlinear systems with uncertainty and external disturbances, the reference [26] uses fuzzy neural networks to approximate unknown nonlinear functions and designs adaptive backstepping fuzzy neural sliding mode controllers. However, the fuzzy rule acquisition method in fuzzy neural networks is complex, and there is also a contradiction between the complexity of the model and the generalization ability. For boost converters containing constant power loads in DC microgrid, without an accurate mathematical model and without stable dynamic systems, a nonlinear control method combining an accurate feedback linearization technique with adaptive backstepping sliding mode control (ABSMC) is proposed in the reference [27]. The method solves the instability problem caused by constant power loads, reduces the impact of sliding mode chattering on the system and ensures the stability of the DC bus voltage. However, the control method does not take into account the regulation of the inductor current, which may cause spikes, or the lack of inertia of the system. Reference [28] designed a nonlinear backstepping sliding mode controller for airship trajectory tracking based on the disturbance observer. Simulation analysis shows that compared with traditional backstepping control and sliding mode control strategies, the proposed method is more robust in the three cases of unknown disturbance, model parameter uncertainty, and wind speed influence. However, the sliding mode control law often introduces the upper bound of the uncertainty term as the control coefficient of the switching function, which is easy to cause high-frequency and high-amplitude chattering of the output control quantity. To avoid this problem, an adaptive algorithm can be used to optimize it [29].

In summary, the main contributions of this paper include: (1) Propose a nonlinear droop control law based on the converter output voltage variation rate $\mathrm{d}V_{\mathrm{dc}}/\mathrm{d}t$, which facilitates the voltage stability of the bus. (2) Propose an adaptive coefficient function that limits the converter output voltage variation rate, which has continuous, smooth, and saturated nonlinear characteristics. (3) Propose a three-level cascade control method that is based on a nonlinear virtual inertia control with droop variable coefficients and adaptive backstepping sliding mode voltage and current double closed-loop control. It achieves robust high stability of bus voltages in distributed multi-source DC microgrid. (4) Verify the feasibility and effectiveness of the proposed method by comparing the results with traditional control methods.

2. DC Microgrid Structure and Modeling

2.1. System Structure and Working Principle

The DC microgrid studied in this paper is shown in Figure 1.

In Figure 1, the main circuit of the microgrid is connected to the DC bus by a plurality of parallel distributed DC power sources V_{s} through a buck–boost converter and a common load R_{L}.

As the main control circuit, the buck–boost converter is composed of a power switch S, a freewheeling diode D, an inductor L, a resistor R, and a capacitor C. V_{dc} and i_{dc} are the output voltage and current of the buck–boost converter, i_L is the current flowing through the inductor L, V_{o} is the DC bus voltage, and $V_{\mathrm{o\,ref}}$ is the voltage reference value set by the DC bus voltage.

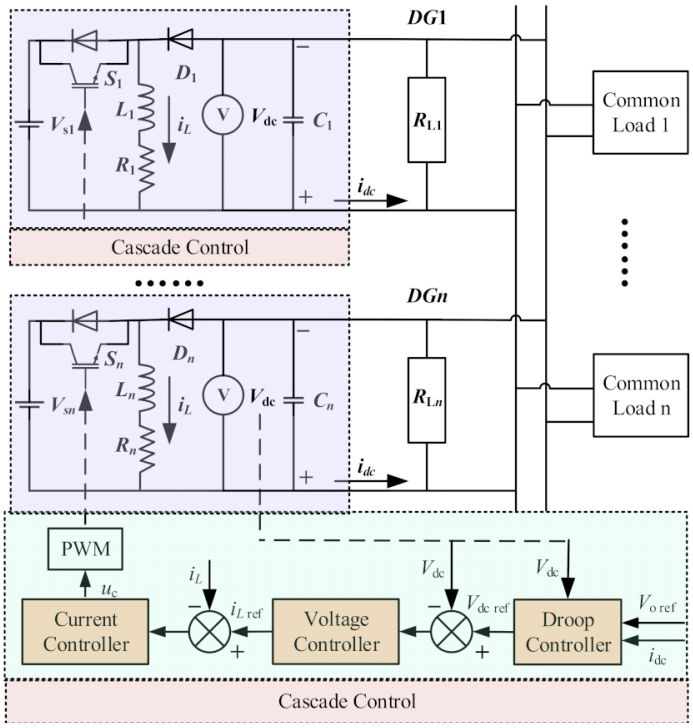

Figure 1. The control structure of the DC microgrid.

In order to coordinate the output power of each buck–boost converter and to maintain the DC bus voltage V_o stable, a three-level cascade control structure consisting of droop control, voltage and current control is used for the PWM drive control of all the converters connected in parallel in the system. To realize the reasonable distribution of converter power and improve the inertia of the converter interface, the droop control adopts a nonlinear virtual inertia controller based on a variable droop coefficient. The controller generates the reference voltage $V_{\mathrm{dc\,ref}}$ of the external voltage control loop. According to the converter output voltage and current deviation, the voltage controller and current controller adopt an adaptive backstepping sliding mode control (ABSMC) method to generate the reference current $i_{L\ \mathrm{ref}}$ of the current loop and the PWM duty cycle control signal of the buck–boost converter power switch u_c. Finally, the stable operation of the DC microgrid is realized.

2.2. Main Circuit Model

According to Figure 1, the buck–boost converter average model can be derived based on the KCL and KVL rules

$$C\frac{\mathrm{d}V_{\mathrm{dc}}}{\mathrm{d}t} = (1-u)i_L - i_{\mathrm{dc}} \tag{1}$$

$$L\frac{\mathrm{d}i_L}{\mathrm{d}t} = -Ri_L - (1-u)V_{\mathrm{dc}} + uV_{\mathrm{s}} \tag{2}$$

where u represents the PWM duty cycle.

Define the state variable $x_1 = V_{\mathrm{dc}}$, $x_2 = \dot{x}_1$, the voltage controller control amount $m_V = \dot{i}_{L\mathrm{ref}}$; $x_3 = i_L$, $x_4 = \dot{x}_3$, the current controller control amount $m_i = \dot{u}_c$. Since the system is in a steady state, $i_{\mathrm{dc}} = V_{\mathrm{dc}}/R_L$, combined with Equations (1) and (2), we get

$$\begin{cases} \dot{x}_1 = x_2 \\ \dot{x}_2 = a_1x_2 + b_1m_V + F_V \end{cases} \tag{3}$$

$$\begin{cases} \dot{x}_3 = x_4 \\ \dot{x}_4 = a_2x_4 + b_2m_i + F_i \end{cases} \tag{4}$$

where $a_1 = -1/R_L C$, $b_1 = (1 - u_c)/C$, $a_2 = -R/L$, $b_2 = (V_{dc} + V_s)/L$. F_V and F_i are respectively the total uncertainty items of the external disturbance of the voltage loop and the current loop.

3. Nonlinear Virtual Inertial Droop Control

3.1. The Principle of the Droop Control

The purpose of droop control is to ensure that the output voltage and current or output voltage and power of the converter run on a given droop characteristic curve. Figure 2 shows a typical *U-I* droop curve.

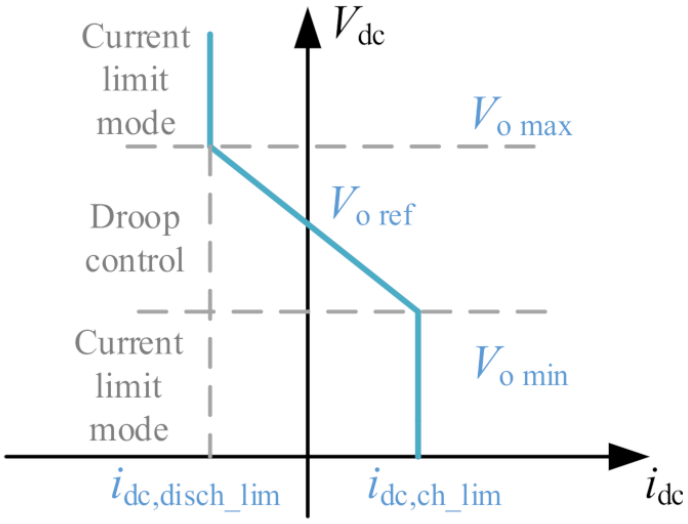

Figure 2. The traditional *U-I* droop curve.

In Figure 2, $V_{o\,max}$ and $V_{o\,min}$ respectively represent the upper and lower bounds of the DC bus voltage operation; $i_{dc,\,ch\_lim}$ and $i_{dc,\,disch\_lim}$ represent the upper and lower bounds of the converter's DC operating current, respectively; $V_{o\,ref}$ represents the longitudinal intercept of the droop curve in mathematical concepts.

The expression of the typical *U-I* droop characteristic is

$$V_{dc\,ref} = V_{o\,ref} - Qi_{dc} \tag{5}$$

where Q is the droop coefficient, which represents the slope of the characteristic curve. It can be equivalent to the virtual impedance of the converter in series in actual control.

According to Equation (5), the change of the output current i_{dc} can immediately cause the corresponding change of the reference output voltage $V_{dc\,ref}$ when the load changes. The buck–boost converter is characterized by low inertia, which makes the bus voltage of the DC microgrid sensitive to the load and susceptible to disturbance. If the coefficient of the droop characteristic can be adjusted with external disturbances, certain inertia can be provided for the system. This can deal with the disturbance of uncertain external factors and can leave a certain margin for the response time of the system.

For this reason, this paper proposes a nonlinear virtual inertia control method based on the variable *U-I* droop coefficient. This method can increase the inertia of the distributed power supply of the buck–boost converter interface and improve the robustness of the bus voltage.

3.2. Nonlinear Virtual Inertia Control Based on Variable Droop Coefficient

The variation curve cluster diagram of the droop coefficient is shown in Figure 3 under different load conditions.

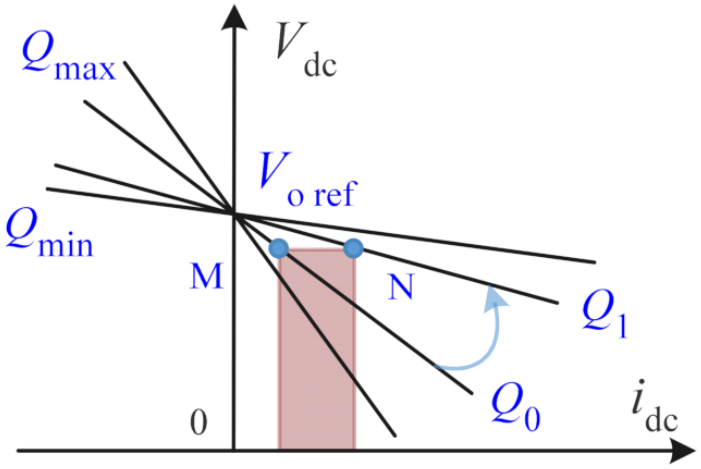

Figure 3. Variation curve clusters of droop coefficients.

Assuming that the system initially operates stably at point M, the original droop coefficient is Q_0. At a certain moment, the system loads suddenly increased. The DC bus capacitor quickly provides auxiliary power support, making the bus voltage stable. Therefore, the operating point of the system will be moved from M to N, and the droop coefficient will be changed from Q_0 to Q_1. The area of the shaded part shown in Figure 3 is the additional power of the converter caused by the change of the droop coefficient. This reflects the positive effect of using fast power compensation to effectively suppress voltage fluctuations.

Thus, a nonlinear variable droop coefficient function with the converter output voltage variation rate $\mathrm{d}V_{dc}/\mathrm{d}t$ is defined as:

$$\tilde{q}\left(\frac{\mathrm{d}V_{dc}}{\mathrm{d}t}\right) = Q_1 + Q_2\frac{\mathrm{d}V_{dc}}{\mathrm{d}t} \tag{6}$$

where Q_1 is the droop coefficient in the steady-state of the system, and Q_2 is the dynamic adjustment coefficient.

Then the *U-I* characteristic expression of the converter based on the variable droop coefficient is

$$V_{dc\ ref} = V_{o\ ref} - \tilde{q}i_{dc} \tag{7}$$

Define the dynamic change Δq of the droop coefficient as

$$\Delta q = Q_2\frac{\mathrm{d}V_{dc}}{\mathrm{d}t} \tag{8}$$

Multiplying both sides of Equation (8) by V_{dc} at the same time, we get

$$\Delta q V_{dc} = Q_2\frac{\mathrm{d}V_{dc}}{\mathrm{d}t}V_{dc} \tag{9}$$

Take the equivalent virtual inertia of the system as C_{vir}. When the load power changes suddenly, causing the current to change Δi, according to the conservation of power, there is

$$\Delta i V_{dc} = C_{vir}V_{dc}\frac{\mathrm{d}V_{dc}}{\mathrm{d}t} \tag{10}$$

Define the ratio of the droop coefficient dynamic change Δq to the current change Δi as $n = \Delta q/\Delta i$, combining Equations (9) and (10), we get

$$\frac{Q_2}{n}V_{dc}\frac{\mathrm{d}V_{dc}}{\mathrm{d}t} = C_{vir}V_{dc}\frac{\mathrm{d}V_{dc}}{\mathrm{d}t} \tag{11}$$

Therefore,

$$C_{vir} = \frac{Q_2}{n} \tag{12}$$

To make the system run stably, it is necessary to limit the value range of the droop coefficient, such as $Q_{min} < \tilde{q} < Q_{max}$. Q_{max}, Q_{min} are respectively the upper and lower limits of the variation range of the droop coefficient.

In this paper, we select the saturation function to limit the dynamic change Δq of the droop coefficient $\tilde{q}$ in Equation (6)

$$g\left(\frac{dV_{dc}}{dt}\right) = \frac{Q_2 \frac{dV_{dc}}{dt}}{\sqrt{1 + \left(Q_2 \frac{dV_{dc}}{dt}\right)^2}} \tag{13}$$

Therefore, we can get a new finite-amplitude variable droop coefficient

$$\tilde{q}\left(\frac{dV_{dc}}{dt}\right) = \begin{cases} Q_1 + (Q_{max} - Q_1) g\left(\frac{dV_{dc}}{dt}\right) \frac{dV_{dc}}{dt} \geq 0 \\ \\ Q_1 + (Q_1 - Q_{min}) g\left(\frac{dV_{dc}}{dt}\right) \frac{dV_{dc}}{dt} < 0 \end{cases} \tag{14}$$

Figure 4 shows the relationship between $\tilde{q}$ in Equation (14) and the converter output voltage variation rate dV_{dc}/dt.

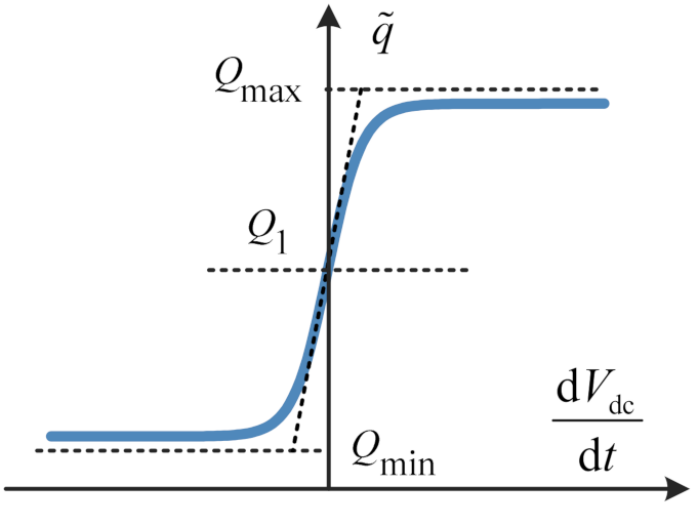

Figure 4. Variation curve of droop coefficient.

When the absolute value of the converter output voltage variation rate dV_{dc}/dt is small, according to the saturation function characteristics, it can be seen from Equation (13) that the curve is approximately a straight line with a fixed slope of Q_2. It can be seen that even if the voltage fluctuation is small, the slope of the droop characteristic can maintain a large fluctuation. Therefore, the proposed nonlinear virtual inertia method can also provide greater inertia for the system. When the absolute value of the converter output voltage variation rate dV_{dc}/dt is large, due to the limitation of the saturation function, the value of $\tilde{q}$ will infinitely approach the upper limit Q_{max} and the lower limit Q_{min} of the droop coefficient variation range without crossing the boundary.

For Equation (14) with finite amplitude variable droop coefficient, we first find its derivative for the converter output voltage variation rate dV_{dc}/dt. Combined with Equations (12) and (13), the equivalent virtual inertia value of the proposed nonlinear variable droop control can be obtained

$$C_{\text{vir}} = \frac{\tilde{q}'}{n} = \begin{cases} \dfrac{Q_2(Q_{\max}-Q_1)}{n\left(1+Q_2^2\left(\frac{\mathrm{d}V_{\text{dc}}}{\mathrm{d}t}\right)^2\right)^{\frac{3}{2}}}\dfrac{\mathrm{d}V_{\text{dc}}}{\mathrm{d}t} \geq 0 \\ \dfrac{Q_2(Q_1-Q_{\min})}{n\left(1+Q_2^2\left(\frac{\mathrm{d}V_{\text{dc}}}{\mathrm{d}t}\right)^2\right)^{\frac{3}{2}}}\dfrac{\mathrm{d}V_{\text{dc}}}{\mathrm{d}t} < 0 \end{cases} \tag{15}$$

According to Equation (15), we can control the value of the virtual inertia C_{vir} of the main circuit of the converter, which can change the inertia of the system. The virtual inertia controller proposed in this paper is used to generate the reference voltage of the external voltage control loop. The virtual inertia control block diagram based on the variable droop coefficient is shown in Figure 5.

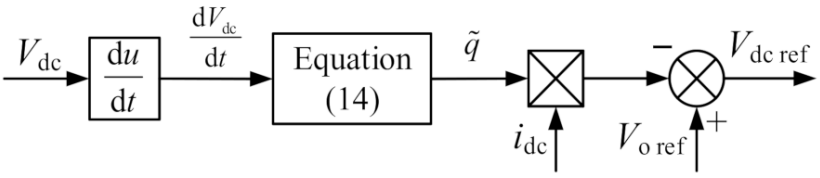

Figure 5. The block diagram of virtual inertia control.

4. Design of Adaptive Backstepping Sliding Mode Controller

In this section, we design a voltage and current double closed-loop controller based on an adaptive backstepping sliding mode method. The adaptive backstepping sliding mode control method is a recursive design method with excellent adaptability. It involves the feedback control method and the judgment of the stability of the Lyapunov function. The proposed controller is designed in multiple steps and is not higher than the order of the system. The sliding mode control method has strong robustness, which limits the uncertainty of the system through the design of the sliding mode. The adaptive backstepping sliding mode control combines the advantages of the adaptive backstepping control method and the sliding mode control method to obtain good dynamic and static performance.

4.1. Design of Backstepping Sliding Mode Controller

According to the cascade control structure shown in Figure 1, the goal of the voltage and current backstepping sliding mode controller is to track the reference input. That is, the output voltage V_{dc} of the converter tracks the given reference voltage $V_{\text{dc ref}}$ output by the previous stage virtual inertia controller. The current i_L flowing through the inductor L of the converter tracks the given reference current $i_{L\ \text{ref}}$ output by the previous stage voltage controller. Ensure that the above two tracking errors tend to zero. The backstepping sliding mode control design mainly includes two steps:

Step 1

Define voltage tracking error z_V and current tracking error z_i as:

$$z_V = V_{\text{dc}} - V_{\text{dc ref}} \tag{16}$$

$$z_i = i_L - i_{L\text{ref}} \tag{17}$$

Define the virtual control variables of voltage tracking error z_V and current tracking error z_i as:

$$\alpha_V = c_1 z_V \tag{18}$$

$$\alpha_i = c_2 z_i \tag{19}$$

where c_1 and c_2 are adjustable design parameters.

Define the Lyapunov functions V_{V1} and V_{i1} as

$$V_{V1} = \frac{1}{2}{z_V}^2 \tag{20}$$

$$V_{i1} = \frac{1}{2}{z_i}^2 \tag{21}$$

Define the new voltage tracking error z_{V1} and current tracking error z_{i1} as:

$$z_{V1} = \dot{z}_V + \alpha_V = \left(\dot{V}_{\mathrm{dc}} - \dot{V}_{\mathrm{dc\ ref}}\right) + c_1(V_{\mathrm{dc}} - V_{\mathrm{dc\ ref}}) \tag{22}$$

$$z_{i1} = \dot{z}_i + \alpha_i = \left(\dot{i}_L - \dot{i}_{L\mathrm{ref}}\right) + c_2(i_L - i_{L\mathrm{ref}}) \tag{23}$$

We can get:

$$\dot{V}_{V1} = z_V \dot{z}_V = z_V z_{V1} - c_1 {z_V}^2 \tag{24}$$

$$\dot{V}_{i1} = z_i \dot{z}_i = z_i z_{i1} - c_2 {z_i}^2 \tag{25}$$

If $z_{V1} = 0$ and $z_{i1} = 0$, then $\dot{V}_{i1} \leq 0, \dot{V}_{V1} \leq 0$. Therefore, this still needs to continue to the next step of design.

Step 2

Further, define the Lyapunov functions V_{V2} and V_{i2} as:

$$V_{V2} = V_{V1} + \frac{1}{2}{\sigma_V}^2 \tag{26}$$

$$V_{i2} = V_{i1} + \frac{1}{2}{\sigma_i}^2 \tag{27}$$

where σ_V and σ_i are respectively the sliding mode surface functions of the voltage controller and current controller, defined as:

$$\sigma_V = k_1 z_V + z_{V1} = \left(\dot{V}_{\mathrm{dc}} - \dot{V}_{\mathrm{dc\ ref}}\right) + (k_1 + c_1)(V_{\mathrm{dc}} - V_{\mathrm{dc\ ref}}) \tag{28}$$

$$\sigma_i = k_2 z_i + z_{i1} = \left(\dot{i}_L - \dot{i}_{L\mathrm{ref}}\right) + (k_2 + c_2)(i_L - i_{L\mathrm{ref}}) \tag{29}$$

where k_1 and k_2 are adjustable design parameters.

$$\begin{aligned} \dot{V}_{V2} &= \dot{V}_{V1} + \dot{\sigma}_V \sigma_V = z_V z_{V1} - c_1 {z_V}^2 + \sigma_V [k_1(z_{V1} - c_1 z_V) \\ &+ a_1\left(z_{V1} + \dot{V}_{\mathrm{dc\ ref}} - \dot{\alpha}_V\right) + b_1 m_V + F_V - \ddot{V}_{\mathrm{dc\ ref}} + \dot{\alpha}_V\Big] \end{aligned} \tag{30}$$

$$\begin{aligned} \dot{V}_{i2} &= \dot{V}_{i1} + \dot{\sigma}_i \sigma_i = z_i z_{i1} - c_2 {z_i}^2 + \sigma_i [k_2(z_{i1} - c_2 z_i) \\ &+ a_2\left(z_{i1} + \dot{i}_{L\mathrm{ref}} - \dot{\alpha}_i\right) + b_2 m_i + F_i - \ddot{i}_{L\mathrm{ref}} + \dot{\alpha}_i\Big] \end{aligned} \tag{31}$$

If $\dot{V}_{i2} \leq 0, \dot{V}_{V2} \leq 0$, the voltage backstepping sliding mode control law $i_{L\ \mathrm{ref}}$ and the current backstepping sliding mode control law u_{c} are designed as:

$$\begin{aligned} i_{L\mathrm{ref}} &= \int m_V \mathrm{d}t = \int b_1^{-1}[-k_1(z_{V1} - c_1 z_V) + \ddot{V}_{\mathrm{dc\ ref}} - \dot{\alpha}_V \\ &- a_1\left(z_{V1} + \dot{V}_{\mathrm{dc\ ref}} - \dot{\alpha}_V\right) - F_V \mathrm{sgn}(\sigma_V) - h_1(\sigma_V + \beta_1 \mathrm{sgn}(\sigma_V))]\mathrm{d}t \end{aligned} \tag{32}$$

$$\begin{aligned} u_c &= \int m_i \mathrm{d}t = \int b_2^{-1}\Big[-k_2(z_{i1} - c_2 z_i) + \ddot{i}_{L,\mathrm{ref}} - \dot{\alpha}_{\ i} \\ &- a_2\left(z_{i1} + \dot{i}_{L,\mathrm{ref}} - \dot{\alpha}_i\right) - F_i \mathrm{sgn}(\sigma_i) - h_2(\sigma_i + \beta_2 \mathrm{sgn}(\sigma_i))]\mathrm{d}t \end{aligned} \tag{33}$$

where h_1, h_2, β_1, β_2 are adjustable design parameters.

4.2. Design of Adaptive Backstepping Sliding Mode Controller

To suppress the influence of the external uncertain disturbance terms F_V and F_i on the voltage and current control links, the sign function coefficients in Equations (32) and (33) often need to be conservatively designed. If we choose the upper bounds of F_V and F_i, it will cause high-frequency chattering of the control law. Therefore, this section uses an adaptive algorithm to estimate F_V and F_i in real-time.

Define the Lyapunov functions V_{V3} and V_{i3} as:

$$V_{V3} = V_{V2} + \frac{1}{2\gamma_1}\tilde{F}_V{}^2 \tag{34}$$

$$V_{i3} = V_{i2} + \frac{1}{2\gamma_2}\tilde{F}_i{}^2 \tag{35}$$

where $\tilde{F}_V$ and $\tilde{F}_i$ are respectively the estimation errors of F_V and F_i, defined as:

$$\tilde{F}_V = F_V{}^* - \hat{F}_V \tag{36}$$

$$\tilde{F}_i = F_i{}^* - \hat{F}_i \tag{37}$$

where $\hat{F}_V$ and $\hat{F}_i$ are respectively the estimated values of F_V and F_i, $F_V{}^*$ and $F_i{}^*$ are the actual values of F_V and F_i, respectively.

$$\begin{aligned}\dot{V}_{V3} &= \dot{V}_{V2} - \tfrac{1}{\gamma_1}\tilde{F}_V\dot{\hat{F}}_V = z_V z_{V1} - c_1 z_V{}^2 + \sigma_V\Big[k_1(z_{V1} - c_1 z_V) + \hat{F}_V - \ddot{V}_{\text{dc ref}} \\ &\quad + a_1\Big(z_{V1} + \dot{V}_{\text{dc ref}} - \dot{\alpha}_V\Big) + b_1 m_V + \dot{\alpha}_V\Big] - \tfrac{1}{\gamma_1}\tilde{F}_V\Big(\dot{\hat{F}}_V - \gamma_1\sigma_V\Big)\end{aligned} \tag{38}$$

$$\begin{aligned}\dot{V}_{i3} &= \dot{V}_{i2} - \tfrac{1}{\gamma_2}\tilde{F}_i\dot{\hat{F}}_i = z_i z_{i1} - c_2 z_i{}^2 + \sigma_i\Big[k_2(z_{i1} - c_2 z_i) + \hat{F}_i - \ddot{i}_{\text{Lref}} \\ &\quad + a_2\Big(z_{i1} + \dot{i}_{\text{Lref}} - \dot{\alpha}_i\Big) + b_2 m_i + \dot{\alpha}_i\Big] - \tfrac{1}{\gamma_2}\tilde{F}_i\Big(\dot{\hat{F}}_i - \gamma_2\sigma_i\Big)\end{aligned} \tag{39}$$

From Equations (34) and (35), if $\dot{V}_{V3} \le 0$, $\dot{V}_{i3} \le 0$, then the adaptive law needs to be designed as:

$$\dot{\hat{F}}_V = \gamma_1\sigma_V \tag{40}$$

$$\dot{\hat{F}}_i = \gamma_2\sigma_i \tag{41}$$

where γ_1 and γ_2 are adjustable design parameters.

The design of the control law consists of determining the equivalent control law for the linear condition of the system and switching control law for the uncertain and disturbance terms. According to Equation (38), the equivalent control law $m_{V\,\text{eq}}$ of the voltage controller is designed as:

$$m_{V\text{eq}} = b_1^{-1}\Big[-k_1(z_{V1} - c_1 z_V) - \hat{F}_V + \ddot{V}_{\text{dc ref}} - a_1\Big(z_{V1} + \dot{V}_{\text{dc ref}} - \dot{\alpha}_V\Big) - \dot{\alpha}_V - h_1\sigma_V\Big] \tag{42}$$

The switching control law $m_{V\,\text{s}}$ is:

$$m_{V\text{s}} = -b_1^{-1}h_1\beta_1\text{sgn}(\sigma_V) \tag{43}$$

Therefore, the voltage control law can be obtained $m_V = m_{V\,\text{eq}} + m_{V\,\text{s}}$

$$m_V = b_1^{-1}\Big[-k_1(z_{V1} - c_1 z_V) - \hat{F}_V + \ddot{V}_{\text{dc ref}} - a_1\Big(z_{V1} + \dot{V}_{\text{dc ref}} - \dot{\alpha}_V\Big) - \dot{\alpha}_V - h_1(\sigma_V + \beta_1\text{sgn}(\sigma_V))\Big] \tag{44}$$

According to Equation (39), the equivalent control law $m_{i\ \mathrm{eq}}$ of the current controller is designed as:

$$m_{i\mathrm{eq}} = b_2^{-1}\left[-k_2(z_{i1} - c_2 z_i) - \hat{F}_i + \ddot{i}_{\mathrm{Lref}} - a_2\left(z_{i1} + \dot{i}_{\mathrm{Lref}} - \dot{\alpha}_i\right) - \dot{\alpha}_i - h_2\sigma_i\right] \tag{45}$$

The switching control law $m_{i\ \mathrm{s}}$ is:

$$m_{is} = -b_2^{-1} h_2 \beta_2 \mathrm{sgn}(\sigma_i) \tag{46}$$

Therefore, the current control law can be obtained $m_i = m_{i\ \mathrm{eq}} + m_{i\ \mathrm{s}}$

$$m_i = b_2^{-1}\left[-k_2(z_{i1} - c_2 z_i) - \hat{F}_i + \ddot{i}_{\mathrm{Lref}} - a_2\left(z_{i1} + \dot{i}_{\mathrm{Lref}} - \dot{\alpha}_i\right) - \dot{\alpha}_i - h_2(\sigma_i + \beta_2 \mathrm{sgn}(\sigma_i))\right] \tag{47}$$

Substituting Equations (38) and (40) into Equation (34),

$$\dot{V}_{V3} = z_V z_{V1} - c_1 {z_V}^2 - h_1 {\sigma_V}^2 - h_1\beta_1|\sigma_V| = -z_1^T Q_1 z_1 - h_1\beta_1|\sigma_V| \le 0 \tag{48}$$

Substituting Equations (39) and (41) into Equation (35),

$$\dot{V}_{i3} = z_i z_{i1} - c_2 {z_i}^2 - h_2 {\sigma_i}^2 - h_2\beta_2|\sigma_i| = -z_2^T Q_2 z_2 - h_2\beta_2|\sigma_i| \le 0 \tag{49}$$

where $z_1^T = \begin{bmatrix} z_V & z_{V1} \end{bmatrix}$, $z_2^T = \begin{bmatrix} z_i & z_{i1} \end{bmatrix}$,

$$Q_1 = \begin{bmatrix} c_1 + h_1 {k_1}^2 & h_1 k_1 - \frac{1}{2} \\ h_1 k_1 - \frac{1}{2} & h_1 \end{bmatrix}, Q_2 = \begin{bmatrix} c_2 + h_2 {k_2}^2 & h_2 k_2 - \frac{1}{2} \\ h_2 k_2 - \frac{1}{2} & h_2 \end{bmatrix}$$

By adjusting the values of h_1, c_1, k_1, h_2, c_2, and k_2, we can make $|Q_1| > 0$, $|Q_2| > 0$. To ensure that it is a positive definite matrix to make the system stable.

Therefore, from Equations (42) and (43), we obtain voltage controller $i_{L\ \mathrm{ref}}$ and current controller u_c as

$$\begin{aligned} i_{\mathrm{Lref}} &= \int m_V \mathrm{d}t = \int b_1^{-1}\left[-k_1(z_{V1} - c_1 z_V) - \hat{F}_V + \ddot{V}_{\mathrm{dc\ ref}}\right. \\ &\left. -a_1\left(z_{V1} + \dot{V}_{\mathrm{dc\ ref}} - \dot{\alpha}_V\right) - \dot{\alpha}_V - h_1(\sigma_V + \beta_1 \mathrm{sgn}(\sigma_V))\right]\mathrm{d}t \end{aligned} \tag{50}$$

$$\begin{aligned} u_\mathrm{c} &= \int m_i \mathrm{d}t = \int b_2^{-1}\left[-k_2(z_{i1} - c_2 z_i) - \hat{F}_i + \ddot{i}_{\mathrm{Lref}}\right. \\ &\left. -a_2\left(z_{i1} + \dot{i}_{\mathrm{Lref}} - \dot{\alpha}_i\right) - \dot{\alpha}_i - h_2(\sigma_i + \beta_2 \mathrm{sgn}(\sigma_i))\right]\mathrm{d}t \end{aligned} \tag{51}$$

5. System Simulation and Analysis

By using the MATLAB/Simulink platform, the correctness of the proposed control method is verified. For the DC microgrid distributed buck–boost converter interface circuit and controller shown in Figure 1, we build models and do experimental analysis. The parameters of the DC microgrid system model are shown in Table 1.

Table 1. The parameters of the DC microgrid system model.

Parameter Name	Numerical Value
DC power supply V_s	100 V
Inductance L	5 mH
Resistance R	0.1 Ω
Capacitance C	4700 μF
Load R_L	200 Ω
PWM switching frequency f_sw	10 kHz
Voltage and current sampling frequency f_sm	10 kHz

The experimental simulation scheme is divided into two types: voltage and current double closed-loop cascade control, and three-level cascade control with virtual inertia. In addition, traditional methods such as voltage and current linear PI control and steady droop control are designed to compare and analyze the new methods in this paper.

5.1. Voltage and Current Double Closed-Loop Cascade Control

This simulation program analyzes the performance of the adaptive backstepping sliding mode current and voltage control method of the buck–boost converter.

It is common that the response of the current inner-loop controller should be much faster than that of the voltage outer-loop controller. Therefore, according to this principle, the parameters of the current inner-loop controller are designed: (1) For ABSMC-based current loop controllers, β_1 can be assumed to be one. (2) If h_1 is too small, the system will go out of control; if h_1 is too large, the time for the system to reach stability will increase significantly. (3) If r_1 is too small, the system will also go out of control; if r_1 is too large, the system will oscillate significantly and it will be difficult to reach stability. (4) If c_1 is too small, the time for the system to reach stability will increase; if c_1 is too large, the overshoot of the output voltage will increase significantly. (5) If k_1 is too small, the system will be out of control; if k_1 is too large, the overshoot of the output voltage will also increase significantly. Therefore, according to the criteria as above, the current controller parameters are designed based on the trial-and-error method. Similarly, the parameter design process for the voltage controller can be completed according to the above steps.

By coordinating and tracking the comprehensive performance of overshoot, response time, and stabilization time, this paper designs an adaptive backstepping sliding mode current and voltage controller parameters, as shown in Table 2.

Table 2. The parameters of the adaptive backstepping sliding mode controller.

Current Control	Parameter Value	Voltage Control	Parameter Value
c_1	20	c_2	0.2
h_1	7.5	h_2	15.5
γ_1	0.1	γ_2	50
β_1	1	β_2	10
k_1	10	k_2	0.1

For comparison, this section designs a buck–boost converter current and voltage PI controller. The design of PI controller parameters is based on the following steps: (1) Establish a PI-based voltage and current double closed-loop controller model in Simulink. (2) Based on the converter switching frequency f_{sw}, the bandwidth of the current control loop should be much smaller than the converter switching frequency f_{sw}, set to $f_{sw}/10$ = 1 kHz; the bandwidth of the voltage control loop should be much smaller than the bandwidth of the current control loop, Set it to $f_{sw}/100$ = 100 Hz. (3) According to the above standards, use the "PID tuning tool" tool to debug the current and voltage double closed-loop PI control parameters as shown in Table 3.

Table 3. The parameters of the current and voltage PI controller.

Current Control	Parameter Value	Voltage Control	Parameter Value
k_{pi}	1.2	k_{pv}	0.45
k_{ii}	0.6	k_{iv}	4.5

At the initial moment of the simulation, set the load R_L = 200 Ω and the bus DC voltage reference value $V_{o\,ref}$ = 0 V. At time 1, 2, and 3 s, $V_{o\,ref}$ suddenly changed to 50, 100, 150 V, respectively; at time 4 s, R_L suddenly changed to 100 Ω.

As shown in Figure 6, when the voltage reference value and load change, this scheme compares the response performance of cascaded PI and cascaded ABSMC. As shown in Figure 6a–e, the proposed cascaded ABSMC is compared with the traditional cascaded PI. In the 1–4 s period, while the response time is accelerated, the overshoot is reduced by about 1.5%, 0.8%, 0.4%, 0.8%, and there is no static error in the steady-state. When tracking the change of the voltage reference value, the proposed control method shows better transient and steady-state performance. Compared with the control method based on cascaded PI, the proposed control method based on cascaded ABSMC reflects lower overshoot, faster response speed, and shorter settling time under the effect of voltage tracking and load disturbance.

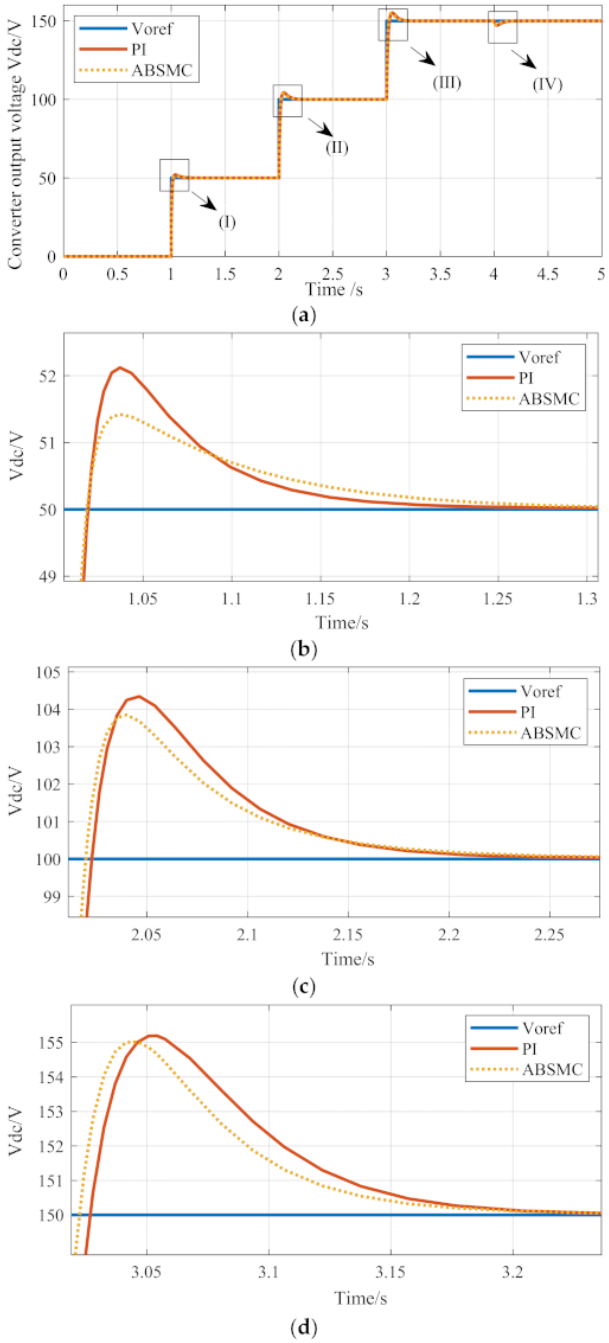

Figure 6. *Cont.*

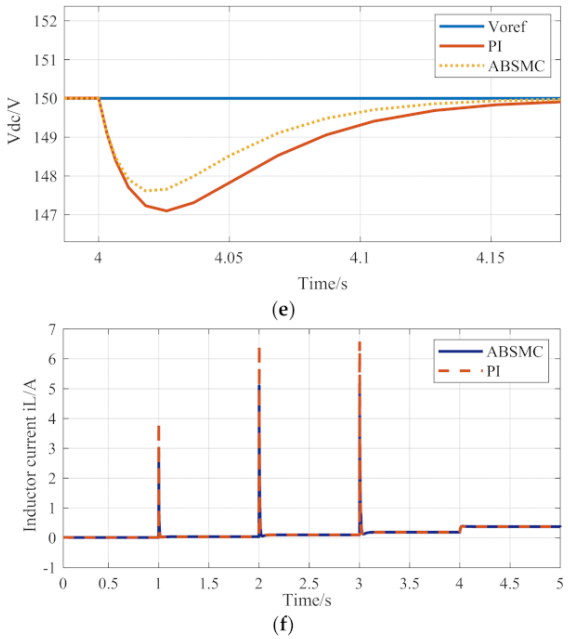

Figure 6. Voltage and current double closed-loop cascade control simulation. (**a**) Converter output voltage response. (**b**) Phase I response. (**c**) Phase II response. (**d**) Phase III response. (**e**) Phase IV response. (**f**) Converter inductor current response.

In addition, as shown in Figure 6f, when the reference value of the bus voltage changes significantly, the peak current of the proposed control method based on cascaded ABSMC is much lower than that of the control method based on cascaded PI. In summary, compared with the traditional control method based on cascaded PI, the proposed control method based on cascaded ABSMC shows better transient and steady-state performance.

5.2. Three-Level Cascade Control with Virtual Inertia

This simulation program analyzes the performance of the proposed three-level cascade control method.

The parameter Q_2 plays an important role in the nonlinear virtual inertia control method based on the variable droop coefficient. To better choose the parameter value of Q_2, this scheme adopts the comparative analysis method to carry out a multi-parameter simulation comparison.

The bus DC voltage reference value $V_{o\,ref}$ is set to change between 150–140 V in the 3rd and 4th seconds, and the Q_2 value is selected as 1, 5, 10, 20, 50, 100 for simulation.

As shown in Figure 7, with the increase of Q_2, when the bus reference voltage changes suddenly, the inertia of the converter output voltage also increases. However, when the reference value of the bus voltage changes, as Q_2 increases, it takes longer for the output reference voltage of the converter to establish a new steady state, which also means that the response speed of the proposed nonlinear virtual inertial control method will be slower.

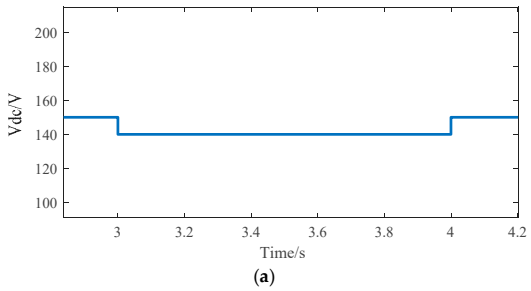

Figure 7. *Cont.*

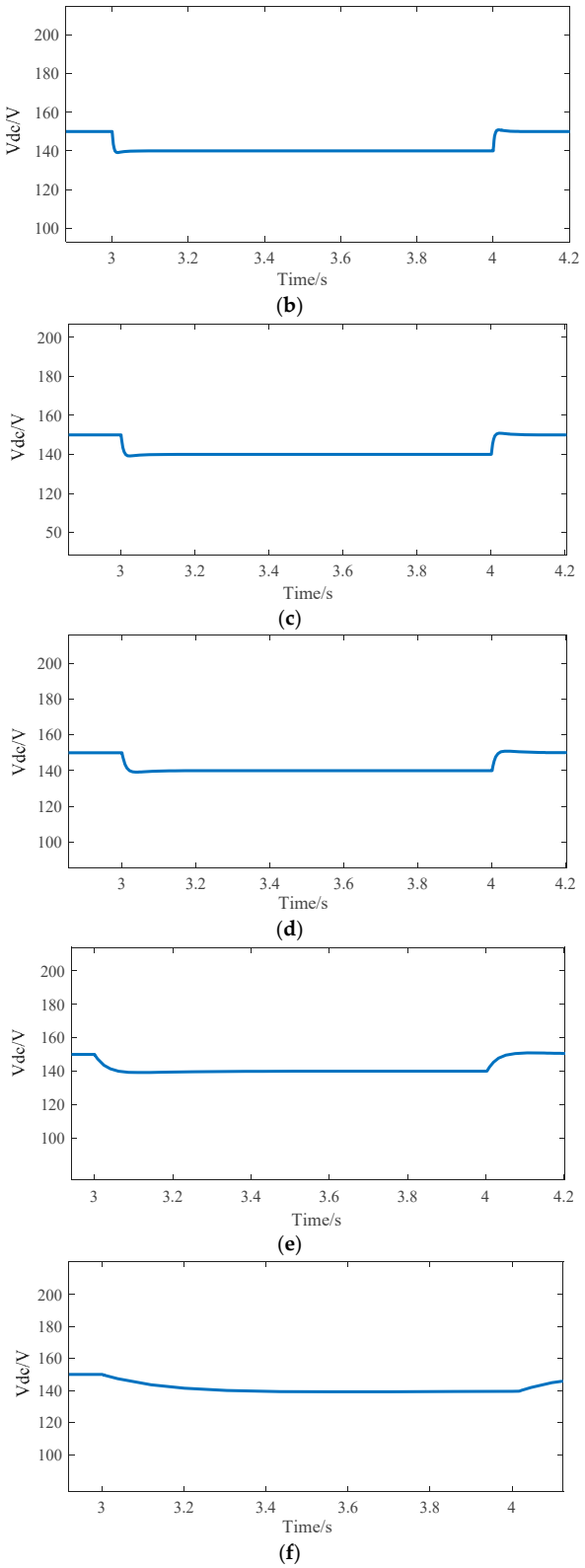

Figure 7. Comparison of response performance of variable droop coefficient. (**a**) $Q_2 = 1$. (**b**) $Q_2 = 5$. (**c**) $Q_2 = 10$. (**d**) $Q_2 = 20$. (**e**) $Q_2 = 50$. (**f**) $Q_2 = 100$.

Based on the above considerations, the parameter value of Q_2 is selected as 25 in this paper. The parameters of the proposed nonlinear virtual inertial droop control method are shown in Table 4.

Table 4. The parameters of the Variable droop coefficient.

Parameter Name	Parameter Value	Parameter Name	Parameter Value
Q_1	7.5	Q_{max}	30
Q_2	25	Q_{min}	15

To verify the performance of the proposed three-level cascade control method, four different cascade control methods are designed for comparison: (i) Traditional droop control and current and voltage PI three-level cascade control (PIdroop); (ii) Virtual inertial droop control and current Voltage PI three-level cascade control (PIVIC); (iii) Traditional droop control and three-level cascade control of current and voltage ABSMC (ABSMCdroop); (iv) Virtual inertia droop control and current and voltage ABSMC three-level cascade control (ABSMCVIC).

To prove that the proposed three-level cascade control with virtual inertia has good tracking characteristics under the reference input step change, this scheme sets the bus DC voltage reference value $V_{o\ ref}$ = 20 V. At 0.5 and 1.5 s moments, $V_{o\ ref}$ respectively suddenly changed to 50 and 100 V; at 2.5 s and 3.5 s moments, $V_{o\ ref}$ respectively suddenly changed to 50 and 20 V.

As shown in Figure 8, the proposed control method shows better transient and steady-state performance when tracking the voltage reference value. Compared to other three-level cascade control methods, the proposed method exhibits lower overshoot, faster response speed and shorter settling time when tracking the voltage reference value.

Considering the impact of load mutation on the bus voltage, this scheme sets the initial time of simulation, load R_L = 200 Ω, bus DC voltage reference value $V_{o\ ref}$ =150 V. At the 3rd second moment, R_L suddenly changes to 100 Ω; at the 4th second moment, R_L suddenly changes to 200 Ω.

Figure 9 shows the output voltage of the converter when the above four different control methods respond to load changes. The performance parameters of four different control methods are shown in Table 5. It can be seen from Table 5 that the proposed three-level cascade control method with virtual inertia shows lower overshoot, shorter transition time and smaller IAE (Absolute error integration indicator) when responding to load changes and provides higher inertia for the output voltage of the converter.

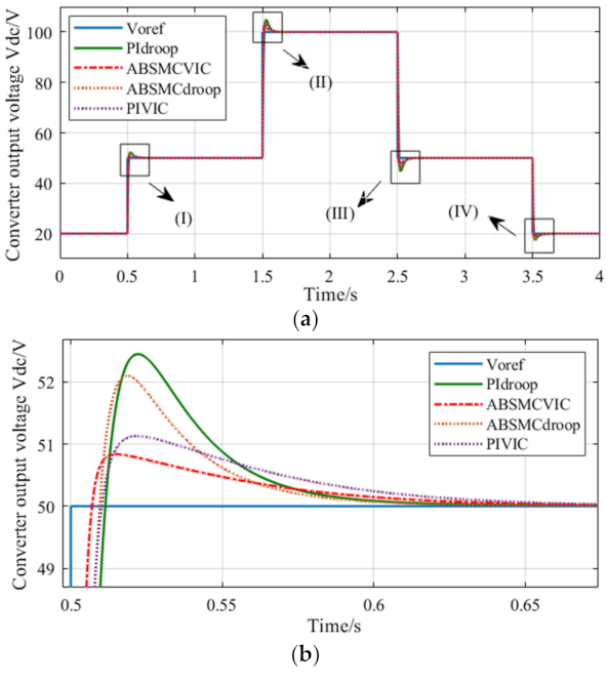

Figure 8. *Cont*.

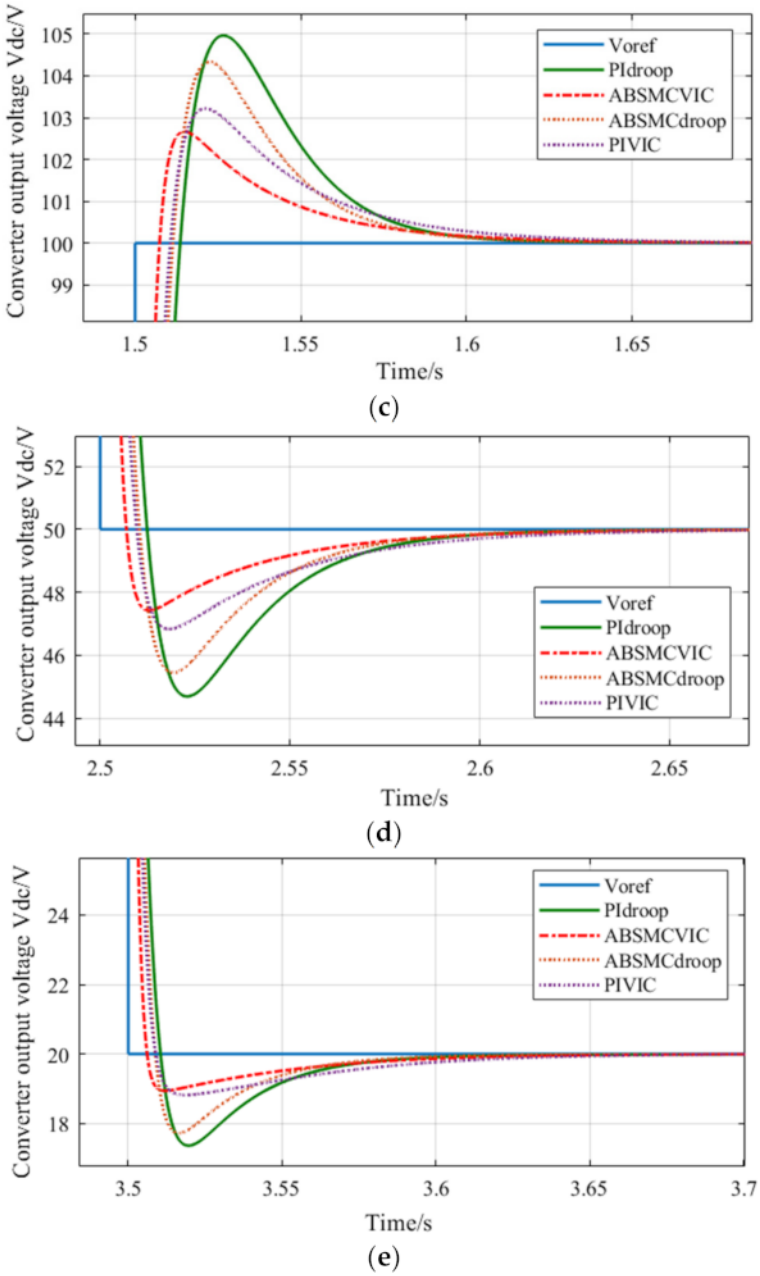

Figure 8. Output voltage response based on three-level cascade control. (**a**) Converter output voltage response. (**b**) Phase I response. (**c**) Phase II response. (**d**) Phase III response. (**e**) Phase IV response.

Table 5. The performance parameters of four different control methods.

Control Strategy	R_L Change to 100 Ω			R_L Change to 200 Ω		
	Overshoot	Transition Time /ms	IAE	Overshoot	Transition Time /ms	IAE
PIdroop	3%	70	0.154	3.13%	70	0.168
PIVIC	2.13%	65	0.1295	2.13%	64	0.129
ABSMCdroop	2.47%	65	0.11	2.6%	64	0.1125
ABSMCVIC	1.47%	60	0.063	1.53%	60	0.0615

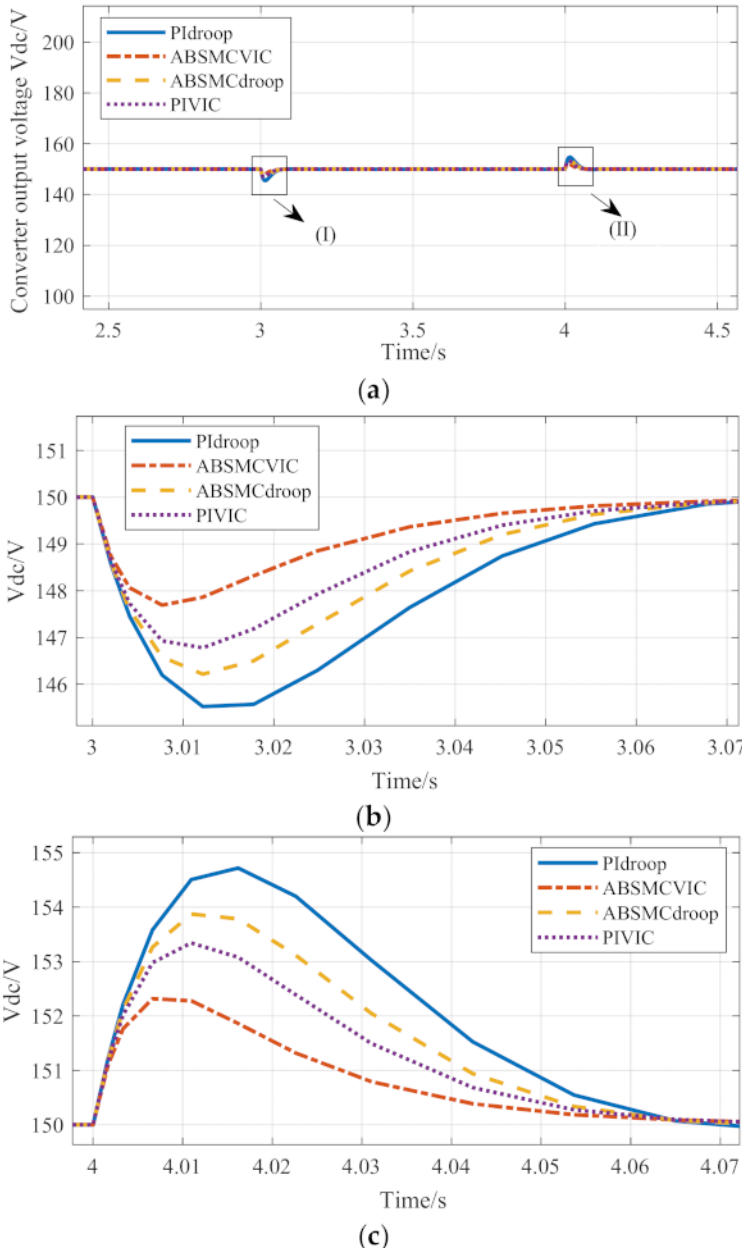

Figure 9. Cascade control method simulation. (**a**) Comparison of response performance of four cascade control methods. (**b**) Phase I comparison waveform. (**c**) Phase II comparison waveform.

5.3. Three-Level Cascade Control under Continuous Dynamic Changes

This scheme sets the voltage reference value $V_{o\,ref}$ to change continuously and dynamically within a small range of 90~110 V and a large range of 50~150 V. Under the three-level cascade control conditions based on virtual inertia droop control and current and voltage adaptive backstepping sliding mode control, the response curve of the converter output voltage V_{dc} is shown in Figure 10.

Figure 10a shows that the converter can track the voltage reference value accurately and achieve effective control of the output voltage when the DC bus voltage reference value $V_{o\,ref}$ varies continuously and dynamically in a small range. Figure 10b shows that due to the capacitance of the capacitor, there is a slight delay in tracking the high-frequency voltage signal. But the trend of the response is consistent with the trend of the original signal of the voltage reference value, and finally tends to be stable.

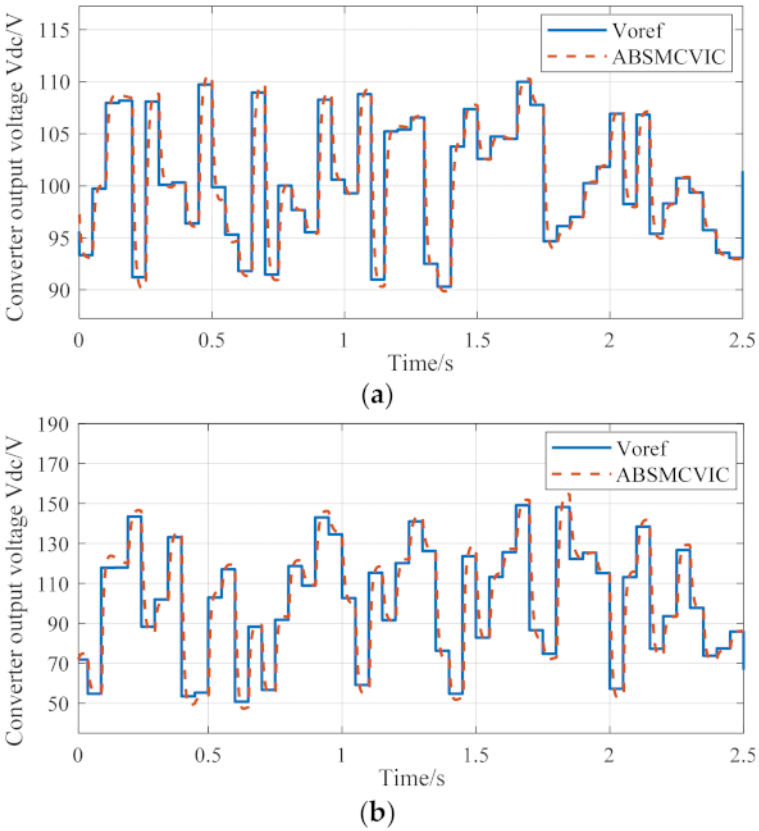

Figure 10. Output voltage response curves of converters under continuous dynamic changes. (**a**) Continuous dynamic change in a small range. (**b**) Continuous dynamic change in a large range.

6. Conclusions

This paper proposes a new cascade control of DC microgrid based on nonlinear virtual inertia and adaptive backstepping sliding mode. Simulation verification shows that, compared with the traditional PI cascade control, the proposed voltage and current double closed-loop control method based on adaptive inversion sliding mode exhibits lower overshoot, shorter stabilization time, with good anti-disturbance, dynamic voltage regulation and steady-state precision control performance. Compared to conventional fixed droop control, the virtual inertia controller based on a nonlinear variable droop coefficient introduces the converter output voltage variation rate feedback term, which provides more flexible and effective inertia for the voltage stability control of the converter. This not only helps the system to withstand source load power shocks, but also improves the robustness of the DC microgrid supply voltage, and further ensures the stability of the system operation.

Author Contributions: Conceptualization, J.M., X.Z. and A.W.; software, X.Z. and T.D.; validation, X.Z. and T.D.; formal analysis, J.M. and C.Y.; investigation, J.M. and A.W.; data curation, J.M. and X.Z.; writing—original draft preparation, X.Z.; writing—review and editing, J.M. and X.Z.; supervision, J.M.; project administration, J.M.; funding acquisition, J.M. and A.W. All authors have read and agreed to the published version of the manuscript.

Funding: This work is supported in part by the Natural Science Research Program of Jiangsu Colleges and Universities under Grant No. 20KJA470002, and Science and Technology Research Program of Nantong Grant No. JC2020094, MS22020022.

Data Availability Statement: The data used to support the findings of this study are available from the corresponding author upon request.

Conflicts of Interest: The authors declare no conflict of interest.

Nomenclature

V_s	Distributed DC power supply	Q_{max}	Upper limit of the variation range of the droop coefficient
V_{dc}	Converter output voltage	Q_{min}	Lower limit of the variation range of the droop coefficient
dV_{dc}/dt	Converter output voltage variation rate	$\tilde{q}$	Variable droop coefficient with finite amplitude
i_{dc}	Converter output current	z_V	Voltage tracking error
i_L	Current flowing through inductor L	z_i	Current tracking error
V_o	DC bus voltage	α_V	Voltage tracking error virtual control volume
$V_{o\ ref}$	DC bus voltage reference value	α_i	Current tracking error virtual control volume
$V_{dc\ ref}$	Reference voltage for voltage control loop	σ_V	Voltage Controller sliding surface switching function
$i_{L\ ref}$	Reference currents for current control loop	σ_i	Current controller sliding surface switching function
u_c	PWM duty cycle control signal	z_{V1}	New voltage tracking error
m_V	Voltage controller control law	z_{i1}	New current tracking error
m_i	Current controller control law	$\tilde{F}_V$	Estimation error of F_V
F_V	Voltage loop uncertainty disturbance term	$\tilde{F}_i$	Estimation error of F_i
F_i	Current loop uncertainty disturbance term	$\hat{F}_V$	Estimated value of F_V
$V_{o\ max}$	DC bus voltage upper boundary	$\hat{F}_i$	Estimated value of F_i
$V_{o\ min}$	DC bus voltage lower boundary	$F_V{}^*$	Actual value of F_V
$i_{dc,\ ch\_lim}$	Converter current upper boundary	$F_i{}^*$	Actual value of F_i
$i_{dc,\ disch\_lim}$	Converter current lower boundary	$m_{V\ eq}$	Equivalent control law of voltage controller
Q_0	Original droop coefficient	$m_{V\ s}$	Switching control law of voltage controller
Q_1	Droop coefficient of the system at steady state	$m_{i\ eq}$	Equivalent control law of current controller
Q_2	System dynamic adjustment coefficient	$m_{i\ s}$	Switching control law of current controller
V_{V1}, V_{V2}, V_{V3}	Voltage controller Lyapunov functions	V_{i1}, V_{i2}, V_{i3}	Current controller Lyapunov functions

References

1. Elavarasan, R.M.; Shafiullah, G.M.; Padmanaban, S.; Kumar, N.M.; Annam, A.; Vetrichelvan, A.M.; Mihet-Popa, L.; Holm-Nielsen, J.B. A Comprehensive Review on Renewable Energy Development, Challenges, and Policies of Leading Indian States with an International Perspective. *J. IEEE Access* **2020**, *8*, 74432–74457. [CrossRef]
2. Nejabatkhah, F.; Li, Y.W.; Tian, H. Power Quality Control of Smart Hybrid AC/DC Microgrids: An Overview. *J. IEEE Access* **2019**, *7*, 52295–52318. [CrossRef]
3. Dragicevic, T.; Lu, X.; Vasquez, J.C.; Guerrero, J. DC Microgrids—Part II: A Review of Power Architectures, Applications, and Standardization Issues. *J. IEEE Trans. Power Electron.* **2016**, *31*, 3528–3549. [CrossRef]
4. Guerrero, J.M.; Vasquez, J.C.; Matas, J.; de Vicuna, L.G.; Castilla, M. Hierarchical control of droop-controlled ac and dc microgrids—A general approach toward standardization. *J. Ind. Electron. IEEE Trans.* **2011**, *58*, 158–172. [CrossRef]
5. Dragicevic, T.; Guerrero, J.; Vasquez, J.C.; Skrlec, D. Supervisory control of an adaptive-droop regulated dc microgrid with battery management capability. *J. IEEE Trans. Power Electron.* **2014**, *29*, 695–706. [CrossRef]
6. Huang, P.-H.; Xiao, W.; El Moursi, M.S. A practical load sharing control strategy for DC microgrids and DC supplied houses. In Proceedings of the IECON 2013-39th Annual Conference of the IEEE Industrial Electronics Societ, Vienna, Austria, 10–13 November 2013; pp. 7124–7128.
7. Manandhar, U.; Wang, B.; Zhang, X.; Beng, G.H.; Liu, Y.; Ukil, A.; Gooi, H.B. Joint Control of Three-Level DC–DC Converter Interfaced Hybrid Energy Storage System in DC Microgrids. *J. IEEE Trans. Energy Convers.* **2019**, *34*, 2248–2257. [CrossRef]
8. Unamuno, E.; Paniagua, J.; Barrena, J.A. Unified Virtual Inertia for ac and dc Microgrids: And the Role of Interlinking Converters. *J. IEEE Electrif. Mag.* **2019**, *7*, 56–68. [CrossRef]
9. D'Arco, S.; Suul, J.A. Equivalence of Virtual Synchronous Machines and Frequency-Droops for Converter-Based MicroGrids. *J. IEEE Trans. Smart Grid* **2014**, *5*, 394–395. [CrossRef]
10. Zhang, X.; Zhong, Q.C.; Ming, W.L. Stabilization of Cascaded DC/DC Converters via Adaptive Series-Virtual-Impedance Control of the Load Converter. *J. IEEE Trans. Power Electron.* **2016**, *31*, 6057–6063. [CrossRef]
11. Mendez-Diaz, F.; Pico, B.; Vidal-Idiarte, E.; Calvente, J.; Giral, R. HM/PWM Seamless Control of a Bidirectional Buck-Boost Converter for a Photovoltaic Application. *J. IEEE Trans. Power Electron.* **2019**, *34*, 2887–2899. [CrossRef]
12. Liu, S.; Xie, X.; Yang, L. Analysis, Modeling and Implementation of a Switching Bi-Directional Buck-Boost Converter Based on Electric Vehicle Hybrid Energy Storage for V2G System. *J. IEEE Access* **2020**, *8*, 65868–65879. [CrossRef]
13. Restrepo, C.; Konjedic, T.; Flores-Bahamonde, F.; Vidal-Idiarte, E.; Calvente, J.; Giral, R. Multisampled Digital Average Current Controls of the Versatile Buck-Boost Converter. *J. IEEE J. Emerg. Sel. Top. Power Electron.* **2019**, *7*, 879–890. [CrossRef]

14. Chandrasekar, B.; Nallaperumal, C.; Padmanaban, S.; Bhaskar, M.S.; Holm-Nielsen, J.B.; Leonowicz, Z.; Masebinu, S.O. Non-Isolated High-Gain Triple Port DC–DC Buck-Boost Converter with Positive Output Voltage for Photovoltaic Applications. *J. IEEE Access* **2020**, *8*, 113649–113666. [CrossRef]
15. Rana, N.; Banerjee, S. Development of an Improved Input-Parallel Output-Series Buck-Boost Converter and Its Closed-Loop Control. *J. IEEE Trans. Ind. Electron.* **2019**, *67*, 6428–6438. [CrossRef]
16. Weng, X.; Zhao, Z.; Chen, K.; Yuan, L.; Jiang, Y. A Nonlinear Control Method for Bumpless Mode Transition in Noninverting Buck-Boost Converter. *J. IEEE Trans. Power Electron.* **2021**, *36*, 2166–2178. [CrossRef]
17. Biricik, S.; Komurcugil, H.; Ahmed, H.; Babaei, E. Super Twisting Sliding-Mode Control of DVR with Frequency-Adaptive Brockett Oscillator. *J. IEEE Trans. Ind. Electron.* **2021**, *68*, 10730–10739. [CrossRef]
18. Sami, I.; Abid, A.; Khan, N.; Zaid, M.M.; Ahmad, H.; Ali, H. Supertwisting Sliding Mode Control of Multi-converter MVDC power systems under constant power loads. In Proceedings of the 2021 IEEE 4th International Conference on Computing, Power and Communication Technologies (GUCON), Kuala Lumpur, Malaysia, 24–29 September 2021; pp. 1–5.
19. Wang, Y.; Ruan, X.; Leng, Y.; Li, Y. Hysteresis Current Control for Multilevel Converter in Parallel-Form Switch-Linear Hybrid Envelope Tracking Power Supply. *J. IEEE Trans. Power Electron.* **2019**, *34*, 1950–1959. [CrossRef]
20. Bellinaso, L.V.; Figueira, H.H.; Basquera, M.F.; Vieira, R.P.; Gründling, H.A.; Michels, L. Cascade Control with Adaptive Voltage Controller applied to Photovoltaic Boost Converters. *J. IEEE Trans. Ind. Appl.* **2019**, *55*, 1903–1912. [CrossRef]
21. Restrepo, C.; Konjedic, T.; Calvente, J.; Milanovic, M.; Giral, R. Fast Transitions Between Current Control Loops of the Coupled-Inductor Buck–Boost DC–DC Switching Converter. *J. IEEE Trans. Power Electron.* **2013**, *28*, 3648–3652. [CrossRef]
22. Feng, Y.; Yu, X.; Han, F. On nonsingular terminal sliding-mode control of nonlinear systems. *J. Autom.* **2013**, *49*, 1715–1722. [CrossRef]
23. Baharizadeh, M.; Golsorkhi, M.S.; Shahparasti, M.; Savaghebi, M. A Two-layer Control Scheme Based on P-V Droop Characteristic for Accurate Power Sharing and Voltage Regulation in DC Microgrids. *J. IEEE Trans. Smart Grid* **2021**, *12*, 2776–2787. [CrossRef]
24. Samanta, S.; Mishra, J.P.; Roy, B.K. Implementation of a virtual inertia control for inertia enhancement of a DC microgrid under both grid connected and isolated operation. *J. Comput. Electr. Eng.* **2019**, *76*, 283–298. [CrossRef]
25. Srinivasan, M.; Kwasinski. A. Control analysis of parallel DC-DC converters in a DC microgrid with constant power loads. *J. Int. J. Electr. Power Energy Syst.* **2020**, *122*, 106207. [CrossRef]
26. Song, S.; Zhang, B.; Xia, J.; Zhang, Z. Adaptive Backstepping Hybrid Fuzzy Sliding Mode Control for Uncertain Fractional-Order Nonlinear Systems Based on Finite-Time Scheme. *IEEE Trans. Syst. Man Cybern. Syst.* **2020**, *50*, 1559–1569. [CrossRef]
27. Wu, J.; Lu, Y. Adaptive Backstepping Sliding Mode Control for Boost Converter with Constant Power Load. *J. IEEE Access* **2019**, *7*, 50797–50807. [CrossRef]
28. Liu, S.Q.; Whidborne, J.F.; He, L. Backstepping sliding-mode control of stratospheric airships using disturbance-observer–ScienceDirect. *J. Adv. Space Res.* **2020**, *67*, 1174–1187. [CrossRef]
29. Liu, S.Q. Adaptive sliding-mode-backstepping trajectory tracking control of underactuated airships. *J. Aerosp. Sci. Technol.* **2020**, *97*, 1–13. [CrossRef]